Domain wall transformations and hopping in $La_{0.7}Sr_{0.3}MnO_3$ nanostructures imaged with high resolution x-ray magnetic microscopy

S Finizio[1], M Foerster[1,2], B Krüger[1], C A F Vaz[1,3], T Miyawaki[4], M A Mawass[1,5], L Peña[1], L Méchin[6], S Hühn[7], V Moshnyaga[7], F Büttner[1,8], A Bisig[1,3,5], L Le Guyader[9], S El Moussaoui[9], S Valencia[10], F Kronast[10], S Eisebitt[8,10] and M Kläui[1]

[1] Institut für Physik, Johannes Gutenberg-Universität, Staudingerweg 7, 55128 Mainz, Germany
[2] ALBA Synchrotron Light Source, Carretera BP 1413, km. 3.3, 08290 Cerdanyola del Valles, Spain
[3] SwissFEL, Paul Scherrer Institut, 5232 Villigen PSI, Switzerland
[4] Department of Crystalline Materials Science, University of Nagoya, 464-8603 Nagoya, Japan
[5] Max-Planck-Institut für Intelligente Systeme, 70569 Stuttgart, Germany
[6] GREYC, UMR 6072, CNRS-ENSICAEN-UCBN, 6 Boulevard du Maréchal Juin, Caen Cedex 14050, France
[7] Georg-August-Universität Göttingen, Friedrich-Hund-Platz 1, 37077 Göttingen, Germany
[8] Institut für Optik und Atomare Physik, Technische Universität Berlin, Straße des 17 Juni 135, 10623 Berlin, Germany
[9] Swiss Light Source, Paul Scherrer Institut, 5232 Villigen PSI, Switzerland
[10] Helmholtz-Zentrum Berlin für Materialien und Energie GmbH, Albert-Einstein-Straße 15, 12489 Berlin, Germany

E-mail: klaeui@uni-mainz.de

Abstract

We investigate the effect of electric current pulse injection on domain walls in $La_{0.7}Sr_{0.3}MnO_3$ (LSMO) half-ring nanostructures by high resolution x-ray magnetic microscopy at room temperature. Due to the easily accessible Curie temperature of LSMO, we can employ reasonable current densities to induce the Joule heating necessary to observe effects such as hopping of the domain walls between different pinning sites and nucleation/annihilation events. Such effects are the dominant features close to the Curie temperature, while spin torque is found to play a small role close to room temperature. We are also able to observe thermally activated domain wall transformations and we find that, for the analyzed geometries, the vortex domain wall configuration is energetically favored, in agreement with micromagnetic simulations.

Keywords: LSMO, current induced domain wall motion, x-ray microscopy

S Online supplementary data available from stacks.iop.org/JPhysD/47/456003/mmedia

1. Introduction

The analysis and manipulation of magnetic domain walls using spin-polarized electrical currents (current-induced domain wall motion, CIDWM and current-induced domain wall transformations) has recently generated much interest, as domain walls and their manipulation can be employed in a wide range of devices [1–3]. Furthermore, spin torque effects can

be exploited as an alternative to the conventional non-scalable approach of field-induced switching [4, 5]. The understanding of the energetics of the domain wall spin structures is of key importance for the application of domain walls in devices [6]. Moreover, a reliable and reproducible domain wall propagation at low current densities still has to be achieved and more complex behaviors, such as the superposition of domain wall displacements and domain wall spin structure changes [7] have to be analyzed in-depth.

In the last years, a series of studies on domain wall configurations and CIDWM in various nanostructured materials has been conducted (for an overview of the recent studies on CIDWM, refer to [8]), albeit primarily concentrating on 3d-ferromagnetic materials, such as Permalloy (Py) [8]. These 3d metal-based materials inherently exhibit a moderate spin polarization, which has prompted research on more advanced metallic materials, such as complex oxide materials with potentially higher spin polarization. A complex oxide material that, thanks to its half-metallic behavior [9] and a Curie temperature of ca. 370 K [10] is of particular interest for device applications at room temperature is the ferromagnetic oxide $La_{0.7}Sr_{0.3}MnO_3$ (LSMO) [11–13]. An additional benefit of this material is the combination of a high spin polarization P and a low saturation magnetization M_s (if compared to standard 3d ferromagnetic materials such as Py), which is promising for CIDWM applications, due to a spin-torque efficiency that scales as P/M_s [14]. A key requirement prior to using this material for domain wall memory or sensing devices are well-defined domain wall spin structures. It has been previously shown that in LSMO nanostructures such well-defined domain walls exist [11, 15]. Moreover it was recently shown that, at low temperatures, highly efficient spin torque effects are present in LSMO [16], which bodes well for using this material. However, this and other similar results were obtained by means of magnetotransport measurements and no direct magnetic domains imaging has been carried out as would be required for the determination of the domain wall spin configuration. Furthermore, in order to probe the thermal stability of this material, heating effects due to the injection of current pulses need to be determined and one needs to ascertain whether the low Curie temperature of LSMO might pose challenges to the use of this material at room temperature. Hence, direct magnetic imaging is necessary to determine changes in the spin structure that can occur due to heating [6] and reveal the energetics of the domain wall spin structures, which are unknown to date.

In this article, we present a magnetic microscopy study of the behavior of the magnetization configurations in LSMO micro- and nanostructured half-ring elements as a function of injected current pulses at room temperature. We observe that the injection of current pulses in the LSMO leads to substantial Joule heating effects, which, by raising the local temperature of the LSMO close to or above its Curie temperature, strongly influence its magnetic configuration. This allows us to analyze the domain wall spin structure transformations to deduce the energetics and find that vortex domain walls are for our geometries the preferred spin structure, in agreement with micromagnetic simulations.

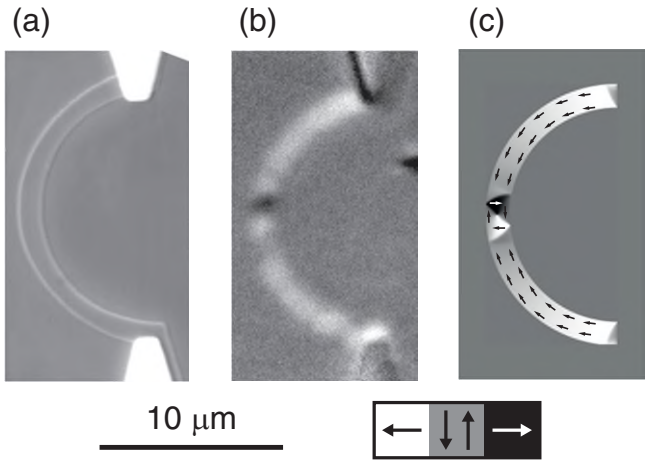

Figure 1. (*a*) Scanning electron micrograph of a 1 μm wide LSMO half-ring structure; (*b*) XMCD-PEEM image of the half-ring structure shown in (*a*), exhibiting a vortex domain wall at the center of the half-ring. (*c*) Micromagnetic simulation of a 1 μm wide LSMO half-ring structure with a vortex domain wall in good agreement with the observations. The black/white arrows indicate the direction of the magnetization.

2. Methodology

The samples analyzed consist of LSMO half-ring structures with widths ranging from 500 nm to 2 μm and a diameter of 10 μm, as shown in figure 1(*a*). The 30 nm thick LSMO film was heteroepitaxially deposited on top of a 45 nm thick $SrTiO_3$ insulation layer homoepitaxially grown on 0.01 wt.% Nb-doped $SrTiO_3$ (1 0 0) (Crystec GmbH) by means of pulsed laser deposition [11] and metalorganic aerosol deposition [17], which yield films with similar materials properties. Following deposition, the LSMO was nanostructured by means of electron beam lithography followed by a chemical etching step. The nanostructures were first lithographically written on the negative resist NLof 2070 (e-beam grade, MicroChem GmbH), then the uncovered areas of the LSMO film were removed by wet chemical etching using a solution of 0.25% H_2O_2 + 0.25% H_2SO_4 in deionized water. This etching solution relies on the reduction of the insoluble Mn(IV) oxide in the LSMO to Mn(II) oxide, soluble in water, according to the following chemical reaction:

$$MnO_2 + H_2O_2 + 2H_3O^+ \rightarrow Mn^{2+} + 4H_2O + O_2.$$

The unprotected LSMO was completely etched away in about 30 s of immersion in the etchant solution (followed by an immediate rinse in deionized water), indicating an etching rate of about 1 nm s^{-1}. As shown in figure 1(*a*), the above described wet chemical etching steps allow for the fabrication of well-defined LSMO nanostructures. 100 nm thick gold electrodes were then patterned on the samples by electron beam lithography, using the positive resist PMMA and its copolymer MMA (MicroChem GmbH), followed by a lift-off step, in order to allow for the injection of electrical pulses across the LSMO half rings.

The imaging of the magnetic configuration of the LSMO half ring structures has been carried out using photoemission

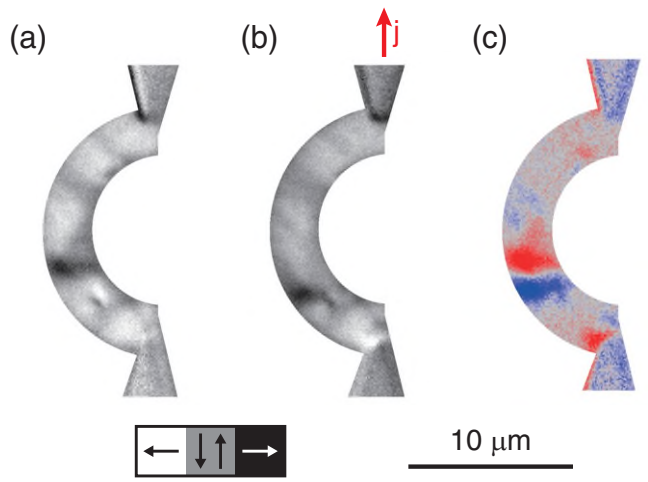

Figure 2. (*a*)–(*b*) XMCD-PEEM image carried out before and after the injection of a 1×10^{11} A m^{-2} pulse burst on a 2 μm wide half-ring LSMO structure; (*c*) difference image obtained subtracting (*a*) from (*b*) showing the displacement of the domain wall. The contrast in the difference image (*c*) allows for the determination of the modifications of the magnetic structure of the LSMO due to the injection of the current pulses.

electron microscopy (PEEM), exploiting the x-ray magnetic circular dichroism (XMCD) effect to achieve magnetic contrast [18]. The energy of the circularly polarized x-rays was tuned to the Mn L_3 edge (642 eV), corresponding to the highest XMCD contrast. An XMCD-PEEM image of an LSMO half-ring structure is shown in figure 1(*b*). Due to the $SrTiO_3$ insulation layer required for injecting the current pulses only across the LSMO half-ring structures without shunting, surface charging upon PEEM imaging occurs. This leads to a lower quality of the acquired images if compared to equivalent images acquired on LSMO nanostructures fabricated on a continuous LSMO thin film by focused-ion-beam lithography or epitaxy lithography [15]. However, as shown in figures 1 and 5, the imaging resolution is still high enough to allow one to distinguish between the different domain wall structures. The XMCD-PEEM imaging was carried out at the SIM (X11MA) beamline at the Swiss Light Source [19, 20] and at the UE49-PGMa beamline at the synchrotron radiation facility (BESSY) of the Helmholtz–Zentrum Berlin [21]. In figure 1(*c*), a micromagnetic simulation of an LSMO half-ring structure is shown. The simulations have been carried out for $T = 0$ K utilizing the MicroMagnum framework [22], using a saturation magnetization $M_s = 2 \times 10^5$ A m^{-1}, an exchange stiffness $A = 1.5 \times 10^{-12}$ J m^{-1} and no magnetocrystalline anisotropy. The numerical discretization utilized in the simulations presented a cell size of 5 nm in the in-plane direction and of 30 nm in the out-of-plane direction (corresponding to the total thickness of the LSMO films studied in the work presented here), with a calculated exchange length of about 7.7 nm.

The LSMO half-ring structures were initialized by applying an in-plane magnetic field of about 50 mT perpendicular to the half-ring structure with an *in-situ* electromagnet, integrated with the PEEM sample holder [23], to obtain a domain wall at the center of the half-ring.

Electrical current pulses were then injected in the LSMO half-ring structures by means of a custom-built electronic setup [23]. For each injection event, a 3-pulse burst with a pulse width of 1 ms and current density varying between 1×10^{10} A m^{-2} and 2×10^{11} A m^{-2} was injected in the LSMO half rings. The magnetic configuration of the LSMO nanostructure was imaged before and after each injection and the displacement of domain walls and changes to the magnetization were determined by analyzing the difference images (i.e. the XMCD image acquired before each injection was subtracted from the corresponding XMCD images acquired after each injection). An example of a difference image, where the contrast in the image allows for a clear identification of changes in the domain wall spin configuration, is shown in figure 2, along with the original XMCD-PEEM images.

3. Results and discussion

By calculating the difference images, the changes of the magnetization configuration in the LSMO structures upon injection of electrical pulses were systematically investigated. As can be observed in figure 3, CIDWM due to a spin transfer torque effect is not the dominating feature upon injection of electrical pulses. Here, an example of a series of difference images is shown, where no clear unidirectional displacement of the domain wall could be detected. Instead, a hopping of the domain wall between different pinning sites in the bottom half of the ring structure is observed. This hopping of the domain wall between the different pinning sites is superimposed with nucleation and annihilation of magnetic domains induced by Joule heating effects, which occur in the top half of the ring structure shown in figure 3.

Such hopping occurs if the energy landscape is sufficiently flat, so that thermal activation can move the domain wall arbitrarily between pinning sites [24]. We have determined the position of the domain walls in the LSMO half ring structures after each injection event and one of these data series is presented in figure 4. We find that at a current density of about 4×10^{10} A m^{-2}, which at low temperatures leads to clear CIDWM [16], the domain wall displacement is dominated by thermally activated hopping at room temperature. Furthermore, nucleation and annihilation events were also observed upon injection of the current pulses. This behavior can be attributed to Joule heating effects due to the injection of the current pulses, which, due to the proximity of the Curie temperature of LSMO to room temperature, lead to a local heating of the LSMO close to or locally above its Curie temperature, thus strongly modifying the magnetic structure of the ferromagnetic material, as previously observed for LSMO nanostructures upon crossing the Curie temperature [15] and dominating over CIDWM effects at room temperature. A slightly different behavior was observed for the domain wall hopping depending on the exact initialization with a magnetic field. We first studied the injection with one current polarity and then with the other polarity and we observe that, upon injection of current pulses with the opposite sign for the current, the movements are different. Such different behavior can be explained by observing that, before each pulse injection sequence, the domain wall configuration of the half-ring was,

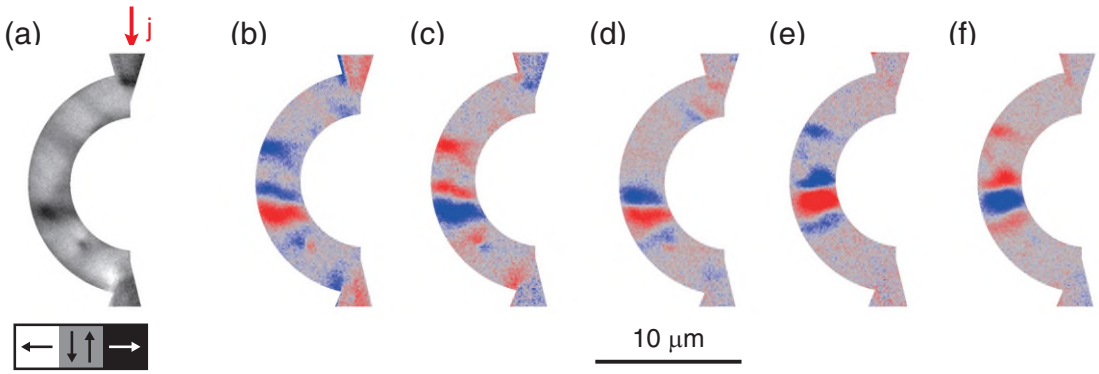

Figure 3. (*a*) XMCD-PEEM image of a 2 μm wide LSMO half-ring structure in the initialized state. (*b*)–(*f*) Difference XMCD-PEEM images calculated after each injection event (current density of 1.2×10^{11} A m^{-2}), showing a hopping of the domain wall between different pinning sites. Contrast away from the domain walls (in this case, on the top half of the ring structure) indicates nucleations and annihilations of domains and domain walls. The red arrow in (*a*) indicates the direction of the current for the injected pulses.

as further explained in the previous section, re-initialized by the application of a magnetic field pulse, which can give rise to slightly different magnetic configurations, with different pinning strengths, making them differently susceptible to thermal activation. Such differences in the behavior after re-initialization with a magnetic field were commonly observed.

The observation of thermally activated hopping and changes in the spin structure of the domain wall now allows us to carry out an analysis of the thermally activated modifications of the magnetic domains and domain walls due to Joule heating, where we estimate the energetics of the domain walls. The first observation is that, after the initialization of the LSMO half rings with a magnetic field, the typically observed domain wall configuration consists in a transverse domain wall, as shown in figure 5(*a*). The injection of the current pulses then changes the domain wall spin structure from transverse to vortex. We find that the injection of current pulses with a current density between 1×10^{10} A m^{-2} and 2×10^{11} A m^{-2} transforms the transverse domain wall into a vortex domain wall, as shown in figure 5(*b*). The vortex domain wall configuration is a much more stable spin structure with respect to the injection of further current pulses. Indeed, we observe that a transformation from a vortex domain wall to another domain wall configuration due to the injection of a current pulse was observed only in about 10% of the injection events (for the analysis presented here, about 10–20 single pulse injection events were analyzed). This indicates that the vortex wall configuration is energetically lower than the transverse wall, while both constitute (meta)stable configurations. Moreover, in contrast to previous observations in Permalloy [6], where only transformations from transverse to vortex walls were observed, in the case presented here also transformations from vortex to transverse domain walls are observed. Analyzing more closely this difference with 3d metal systems, we find that, if a vortex wall configuration is present, in 80% of the cases in which the injection of a current pulse changes the spin configuration of the vortex wall (i.e. in about 8% of the injection events for the vortex domain wall configuration), the domain configuration changes back to a transverse wall configuration. In the remaining cases where the spin structure changes, we observe a transformation to more complex domain wall configurations, such as double vortex walls. This means that the energy of the two domain wall configurations is comparable and that the two configurations are thermally accessible from one another at

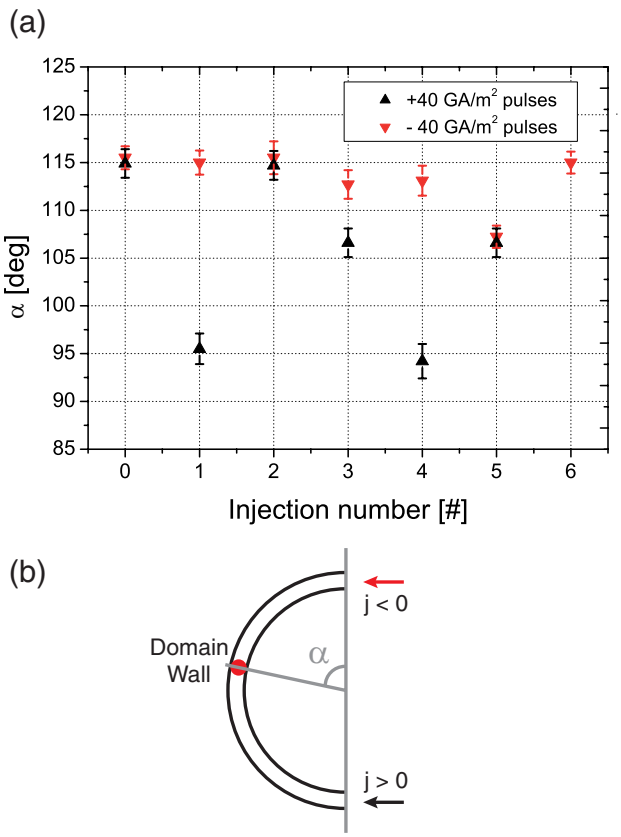

Figure 4. (*a*) Position of the domain wall center in a 2 μm wide LSMO half-ring structure after a series of injections of pulses of 4×10^{10} A m^{-2}. The black upward triangles and the red downward triangles refer to two different injection series. The half-ring structure was initialized by a magnetic field before each series of injections. The sign of the current density refers to the convention illustrated in (*b*), where the arrows indicate the direction of the current; (*b*) sketch of an LSMO half-structure, illustrating the angle convention (α) and sign for the current density for the data points presented in (*a*). The single XMCD-PEEM images employed to generate the data in (*a*) are shown in the supplementary data (stacks.iop.org/JPhysCM/26/456003/mmedia).

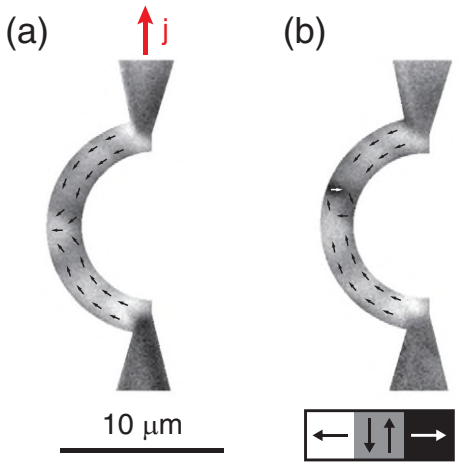

Figure 5. (*a*) XMCD-PEEM image of a 2 μm wide LSMO half-ring structure following the initialization, presenting a transverse domain wall configuration; (*b*) XMCD-PEEM image of the same half-ring structure, after the injection of a 3×10^{10} A m^{-2} pulse burst, showing that the domain wall configuration has changed from transverse to vortex. The red arrow indicates the direction of the current for the injected pulses and the black/white arrows indicate the direction of the magnetization.

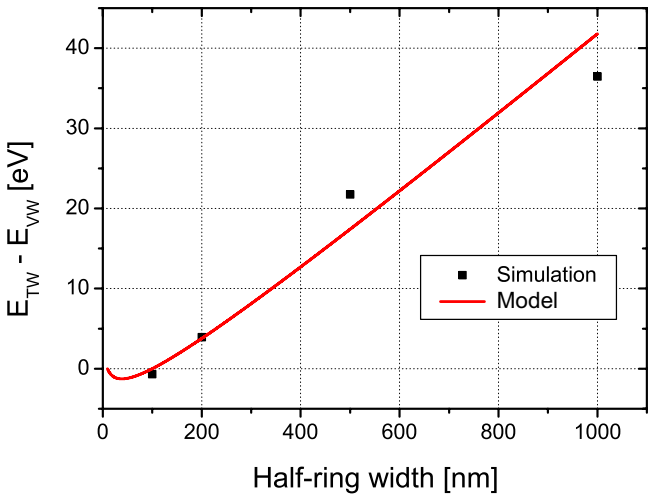

Figure 6. Difference of the domain wall energies between the transverse (TW) and vortex (VW) wall configurations for half-rings of varying widths and a diameter of 10 μm. As can be observed, the vortex wall configuration is favorable for widths above about 100 nm.

room temperature. Within the investigated geometry range (widths of the LSMO half-ring structures between 500 nm and 2 μm), no significant difference in the statistics of the domain wall transformations is observed. A selection of XMCD-PEEM images for different geometries, showing the described domain wall modifications, are presented in the supplementary data (stacks.iop.org/JPhysCM/26/456003/mmedia).

The observation that the vortex wall configuration lies at a lower energy than the transverse wall configuration (for the investigated geometry range) is further backed by micromagnetic simulations of the LSMO half-ring structures. Such simulations have confirmed that the energy of the transverse domain wall configuration is higher than that of the vortex domain wall configuration for widths of the half-ring structure above about 100 nm, as can be observed in figure 6, where the difference between the energy of the simulated transverse and vortex domain wall configurations is plotted.

The energy difference between the simulated transverse and vortex wall configurations plotted in figure 6 has been fitted with the function $E(w) = a \cdot w - b \cdot \log(w) + c$, being E the energy difference between the transverse and vortex wall configurations, w the width (expressed in nm) of the half-ring structure, a and b defined as described in the following sentences and c an additional fitting parameter, describing the energy of the vortex core for the vortex domain wall configuration. Such fitting function has been determined with a 1D model for the energy of the transverse domain wall configuration and a simplified model for the vortex domain wall configuration [25, 26], where it is also possible to observe that the parameters a and b (which allow, respectively, for the determination of the energy of the transverse and vortex domain wall configurations) are defined by $a = 4t\sqrt{A \cdot K}$ and $b = 2\pi \cdot A \cdot t$, where t is the thickness of the LSMO thin film, A the exchange stiffness and K the magnetic anisotropy term (in the case presented here, K is given by the shape anisotropy term). In general, the anisotropy term K depends on the aspect ratio (i.e. the width) of the half-ring structure, thus implying a dependence of the parameter a on the width of the half-ring structure. It is possible to analytically describe the dependence of the anisotropy term on the aspect ratio with the model described in [27]. Taking this dependence into account, we are able to fit the simulated data points presented in figure 6. The simulated behavior then allows us to observe that the vortex wall configuration has a lower energy than the transverse wall configuration for widths of the half-ring structure above 100 nm and, for widths below 100 nm, the resulting energies of the two configurations become comparable. For widths below about 50 nm, the simulated vortex domain wall structures are unstable, as the dimension of the vortex core becomes similar to the width of the half-ring structure. We note that these calculations are carried out for the 0 K values of the magnetic properties. At higher temperatures, both M_s and the exchange will be reduced, so qualitatively the energetic dependence between the transverse and vortex wall configurations will be similar (albeit, quantitatively, the exact values for the energy difference might change). However, we image the magnetization well below the Curie temperature and, for these temperatures, the results of figure 6 are expected to hold, making transverse walls energetically favorable only for structures with widths less than about 100 nm. Thus, for the geometries that were employed in the experiments presented here, the vortex wall has indeed the lowest energy, confirming our experimental observations.

4. Conclusions

In conclusion, we find that, at room temperature, the injection of current pulses into LSMO half-ring nanostructures causes Joule heating effects that, even at relatively low current densities (i.e. $\leqslant 1 \times 10^{11}$ A m^{-2}), are important, due

to the proximity of the Curie temperature of LSMO to room temperature. These thermally-activated events include nucleation and annihilation of domains and domain walls, hopping of the domain walls between different pinning sites and in particular domain wall spin structure transformations. Two (meta-)stable domain wall configurations are observed: transverse and vortex walls. Transverse walls are favored after the initialization of the LSMO half-ring structures with a magnetic field, while vortex domain walls appear due to thermally activated transformations caused by the injection of current pulses due to their lower energy with respect to transverse walls. Furthermore, transformations back to transverse walls are observed, showing that in this material both domain wall configurations are thermally accessible from one another at room temperature.

The results presented here show that Joule heating effects are conspicuous at room temperature, dominating over CIDWM due to spin torque in LSMO, even at current densities where spin torque effects are observed in domain wall motion at low temperatures [16]. In order to render this system more appropriate for CIDWM, one would need to enhance the LSMO thin film quality and its lithographical processing, to reduce the density of magnetic pinning sites and use shorter pulses to reduce heating effects. The above described improvements could then present possible avenues for the usage of this material in spin-torque based devices, while its modest Curie temperature makes this material an ideal playground to study thermal effects.

Acknowledgments

Part of this work was performed at the Swiss Light Source, Paul Scherrer Institut, Villigen, Switzerland and at the Helmholtz–Zentrum Berlin, Germany. The authors further acknowledge the financial support by EU's 7th Framework Programme IFOX (Grant No. NMP3-LA-2010 246102), WALL (Grant No. FP7-PEOPLE-2013-ITN 608031) and MAGWIRE (Grant No. FP7-ICT-2009-5 257707), the European Research Council through the Starting Independent Researcher Grant MASPIC (Grant No. ERC-2007-StG 208162), the Swiss National Science Foundation, the Graduate School of Excellence 'Materials Science in Mainz' (Grant No. GSC 266) and the Deutsche Forschungsgemeinschaft (DFG).

References

[1] Parkin S S P, Hagayashi M and Thomas L 2008 *Science* **320** 190
[2] Cowburn R S 2007 *US Patent* No WO/2007/132174
[3] Diegel M, Glathe S, Mattheis R, Scherzinger M and Halder E 2009 *IEEE Trans. Magn.* **45** 3792
[4] Yamaguchi A, Ono T, Nasu S, Miyake K, Mibu K and Shinjo T 2004 *Phys. Rev. Lett.* **92** 077205
[5] Kläui M, Vaz C A F, Bland J A C, Wernsdorfer W, Faini G, Cambril E and Heyderman L J 2003 *Appl. Phys. Lett.* **83** 105
[6] Laufenberg M *et al* 2006 *Appl. Phys. Lett.* **88** 052507
[7] Heyne L *et al* 2008 *Phys. Rev. Lett.* **100** 66603
[8] Boulle O, Malinowski G and Kläui M 2011 *Mater. Sci. Eng.* R **72** 159
[9] Park J H, Vescovo E, Kim H J, Kwon C, Ramesh R and Venkatesan T 1998 *Nature* **392** 794
[10] Honer G H and van Santen J H 1950 *Physica* **16** 337
[11] Rhensius J *et al* 2011 *Appl. Phys. Lett.* **99** 062508
[12] Cibert J, Bobo J F and Lüders U 2005 *C. R. Phys.* **6** 977
[13] Vaz C A F, Ahn C H and Henrich V E 2009 *Spin-Polarization Effects in Oxide Materials* ed A Hirohata and Y Otani (Kerala: Research Signpost) p 145
[14] Thiaville A, Nakatani Y, Miltat J and Suzuki Y 2005 *Europhys. Lett.* **69** 990
[15] Heidler J *et al* 2012 *J. Appl. Phys.* **112** 103921
[16] Foerster M *et al* 2014 *Appl. Phys. Lett.* **104** 072410
[17] Moshnyaga V, Khoroshun I, Sidorenko A, Petrenko P, Weidinger A, Zeitler M, Rauschenbach B, Tidecks R and Samwer K 1999 *Appl. Phys. Lett.* **74** 2842
[18] Stöhr J, Wu Y, Hermsmeier B D, Samant M G, Harp G R, Koranda S, Dunham D and Tonner B P 1993 *Science* **258** 658
[19] Flechsig U, Nolting F, Fraile-Rodriguez A, Krempasky J, Quitmann C, Schmidt T, Spielmann S and Zimoch D 2010 *AIP Conf. Proc.* **1234** 319
[20] Guyader L L, Kleibert A, Fraile Rodríguez A, Moussaoui S E, Balan A, Buzzi M, Raabe J and Nolting F 2012 *J. Electron Spectrosc. Relat. Phenom.* **185** 371
[21] Kronast F, Schlichting J, Radu F, Mishra S, Noll T and Durr H 2010 *Surf. Interface Anal.* **42** 1532
[22] Code available at http://micromagnum.informatik.uni-hamburg.de/
[23] Heyne L, Kläui M, Rhensius J, Guyader L L and Nolting F 2010 *Rev. Sci. Instrum.* **81** 113707
[24] Eltschka M *et al* 2010 *Phys. Rev. Lett.* **105** 056601
[25] Michael R M and Donahuhe M 1997 *IEEE Trans. Magn.* **33** 4167
[26] Nakatani Y, Thiaville A and Miltat J 2005 *J. Magn. Magn. Mater.* **290** 750
[27] Aharoni A 1998 *J. Appl. Phys.* **83** 3432